Cell, Vol. 90, 217–224, July 25, 1997, Copyright ©1997 by Cell Press

A Model for the Microtubule-Ncd Motor Protein Complex Obtained by Cryo-Electron Microscopy and Image Analysis

Hernando Sosa,* D. Prabha Dias,* Andreas Hoenger,* Michael Whittaker,* Elizabeth Wilson-Kubalek,* Elena Sablin,‡ Robert J. Fletterick,‡ Ronald D. Vale,†‡ and Ronald A. Milligan*§
*Department of Cell Biology MB25
The Scripps Research Institute
10550 North Torrey Pines Road
La Jolla, California 92037
†The Howard Hughes Medical Institute
‡Departments of Biochemistry
and Cellular and Molecular Pharmacology
University of California
San Francisco, California 94143

Summary

Kinesin motors convert chemical energy from ATP hydrolysis into unidirectional movement. To understand how kinesin motors bind to and move along microtubules, we fit the atomic structure of the motor domain of Ncd (a kinesin motor involved in meiosis and mitosis) into three-dimensional density maps of Ncd–microtubule complexes calculated by cryo-electron microscopy and image analysis. The model reveals that Ncd shares an extensive interaction surface with the microtubule, and that a portion of the binding site involves loops that contain conserved residues. In the Ncd dimer, the microtubule-bound motor domain makes intimate contact with its partner head, which is dissociated from the microtubule. This head–head interaction may be important in positioning the dissociated head to take a step to the next binding site on the microtubule protofilament.

Introduction

Kinesin motors belong to a growing family of more than 70 proteins that are involved in organelle transport, chromosome movement during mitosis and meiosis, and spindle formation (for recent reviews, see Bloom and Endow, 1995; Moore and Endow, 1996). Like the other known molecular motors (dyneins and myosins), kinesins use the energy of ATP hydrolysis to move along cytoskeletal filaments (Howard, 1996). Kinesins and dyneins translocate along microtubules, while myosins move along actin filaments.

The best characterized members of the kinesin superfamily are conventional kinesin, an organelle transport motor, and Ncd, a motor involved in meiotic and mitotic spindle formation. Kinesin and Ncd are each composed of two identical motor subunits that are held together by α-helical coiled-coil interactions. However, the architecture and motility properties of these two motors differ significantly from one another. Kinesin is a microtubule plus-end-directed motor (Vale et al., 1985) that has its motor domain at the N terminus of the polypeptide chain (Yang et al., 1989, 1990). Ncd, in contrast, is a microtubule minus-end-directed motor (McDonald et al., 1990; Walker et al., 1990) that has its motor domain at the C terminus of the chain (McDonald and Goldstein, 1990). The factors that govern directionality are unknown, although the position of the motor domain with respect to the entire polypeptide chain does not seem to be the determining factor (Stewart et al., 1993).

A central problem in biological motility is understanding the mechanism of energy transduction by motor proteins at the molecular level. In the case of actomyosin, crystal structures of both actin and myosin have been obtained and incorporated into three-dimensional (3-D) electron image maps of the actomyosin complex to obtain an atomic model of how the motor and actin polymer interact (Rayment et al., 1993). This structural information forms the basis for hypotheses about the energy transduction mechanism in this system (Rayment et al., 1993, 1996).

For microtubule motors, the crystal structures of the motor domains of kinesin (Kull et al., 1996) and Ncd (Sablin et al., 1996) have recently been determined. Even though kinesin and Ncd move in opposite directions along microtubules, their 3-D structures are very similar. Surprisingly, the kinesin structure is also very similar to the catalytic core of the myosin motor. Thus, even though kinesin and myosin bind to different polymers, these molecular motors may share similarities in their mechanisms of mechanochemical transduction.

In order to understand kinesin's mechanism of motility, it is important to know not only the atomic structure of the motor, but also how it binds to microtubules. However, a detailed structural model for the kinesin–microtubule interaction has not been described. To address this problem, we have oriented the recently solved high resolution structure of the Ncd motor domain (Sablin et al., 1996) into 3-D maps of microtubule–Ncd complexes obtained by cryo-electron microscopy (cryo-EM) and image analysis. This approach is similar to the one used to obtain an atomic model of the actomyosin interaction (Rayment et al., 1993). Based on our results, we have identified regions in the bound Ncd motor domain that are likely to interact with microtubules, as well as possible contact sites with the second motor domain in the microtubule-bound Ncd dimer.

Results

Images and Image Analysis

Microtubules polymerized in vitro are composed of variable numbers of protofilaments. Under the assembly conditions used here, 5%–10% of the microtubules contain 15 protofilaments and can be identified in images by their diameter and by the characteristic moiré pattern resulting from the protofilament supertwist (Figures 1a, 1c, and 1e) (Mandelkow and Mandelkow, 1985; Chrétien and Wade, 1991). In diffraction patterns from these microtubules (Figures 1b, 1d, and 1f), the relative positions of intensity peaks near 1/40 $Å^{-1}$ indicate that the tubulin dimers are arranged in 2-start helical paths,

§To whom correspondence should be addressed.

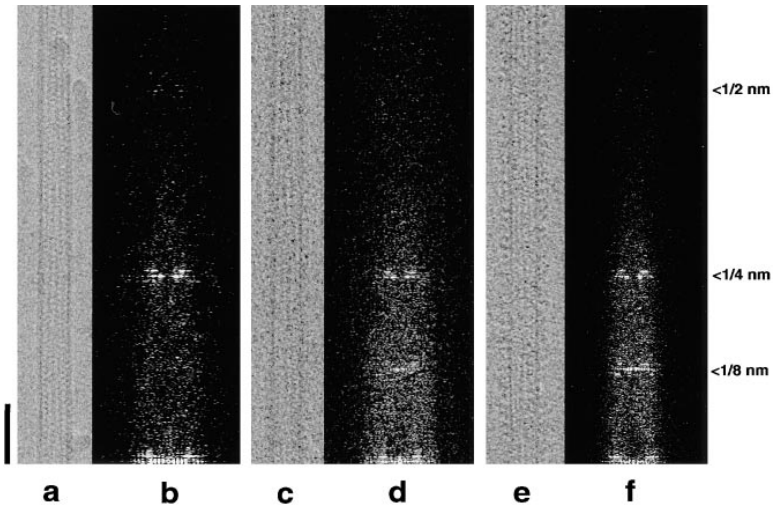

Figure 1. Images and Diffraction Patterns

Cryo-electron micrographs of an undecorated 15 protofilament microtubule (a) and microtubules decorated with recombinant monomeric (c) and dimeric (e) Ncd motors. Only a short portion (~2 moiré repeats) of each microtubule is shown. Images with 4–8 moiré repeats were used in the analysis. The top halves of the corresponding diffraction patterns are shown in (b), (d), and (f), respectively. The equatorial (horizontal) scale of the diffraction patterns is compressed by a factor of 8 for display. Image scale bar is 500 Å.

unlike microtubules with the other commonly found protofilament numbers that contain one or more discontinuities or seams in the helix (Sosa and Milligan, 1996; Sosa et al., 1997). To confirm the helical packing in the filaments that were selected for further analysis, we used back-projection methods (Wade et al., 1995; Sosa and Milligan, 1996; Sosa et al., 1997) to demonstrate that they are indeed helical and do not contain seams (data not shown).

We then analyzed the selected images of undecorated microtubules (Figure 1a) and microtubules decorated with monomeric Ncd (R335-K700) (Figure 1c) and dimeric Ncd proteins (D250-K700) (Figure 1e) by standard helical methods (DeRosier and Moore, 1970; Whittaker et al., 1995; Carragher et al., 1996). To improve the signal-to-noise ratio in the final three maps calculated, we combined 24–46 data sets, representing data averaging over ~12,000–~31,000 asymmetric units (see Table 1). Layer lines to 1/20 $Å^{-1}$ were detected in the final data sets. As is seen in the diffraction patterns from individual images (Figure 1), this layer line was considerably stronger in the undecorated microtubule data than in either of the decorated microtubule data sets.

Table 1. Summary of Parameters Associated with the 3-D Maps

3-D Map	MT	MT-M	MT-D
No. data sets	26	24	46
No. asymm. units averaged	17,476	12,235	30,840
Average phase residual	27.3°	19.1°	17.4°
Average up/down difference	29.0°	32.4°	26.7°

No. data sets is the number of independent near and far data sets averaged to give the final 3D maps. No. asymm. units is the number of asymmetric units (e.g., tubulin dimers) in the average. Average phase residuals were calculated by comparing each raw data set with the final average. Average up/down difference is the average phase difference obtained when the data sets were compared with the final average with the correct and the incorrect polarity, e.g., the average residual for the MT data with the wrong polarity was 56.3° (27.3° + 29.0°). The high values for the average up/down difference mean that undecorated and decorated microtubules have well-defined polarity.

Three-Dimensional Maps

The final 3-D maps of the microtubule (MT) and the microtubule decorated with monomeric (MT-M) and dimeric (MT-D) constructs of Ncd are shown as surface representations and end-on projections in Figure 2. Protofilaments in the MT map have a smooth outer surface and a more rugged inner surface where the tubulin monomers can be recognized as separate units that bulge laterally to make interprotofilament contacts (Amos and Klug, 1974; Hoenger et al., 1995; Kikkawa et al., 1995). When viewed from the plus end (Figure 2, top right), the tubulin monomers exhibit a counterclockwise slew (Sosa and Milligan, 1996). In the MT-M map, the monomeric Ncd motor domain can be identified as an asymmetric density on the outside of the microtubule that tapers toward the microtubule plus end. Viewed from the side (Figure 2, center left), the bound motor domain has a roughly triangular profile and is oriented with its long axis approximately parallel to the microtubule axis. The Ncd–tubulin interaction site lies on the crest of the protofilament, slightly offset vertically with respect to the interprotofilament connections. As described previously (Hoenger et al., 1995; Hoenger and Milligan, 1997), each motor domain makes contact with two tubulin monomers in the protofilament. The view from the plus end illustrates the clockwise slew of the attached motor domain (Figure 2, center right).

In the MT-D map, two similar morphological units are distinguishable on the outside of the microtubule (Figure 2, bottom left) and correspond to the two motor domains of the dimer. One unit interacts with the microtubule (head 1) and is similar to the monomeric motor domain visualized in the MT-M map. The second unit (head 2) is bound with a counterclockwise slew to head 1 (viewed from the plus end, Figure 2, bottom right) and does not interact with the microtubule. Although head 2 is slightly smaller and shows fewer features than head 1, a similar triangular profile can be recognized in side views (Figure 2, bottom left). The long axis of head 2 is rotated by ~45° relative to the long axis of head 1.

Despite the slight differences in the two heads, the map density attributable to head 2 is comparable to that of head 1. As any variability in the position of the detached heads would lead to severe attenuation of

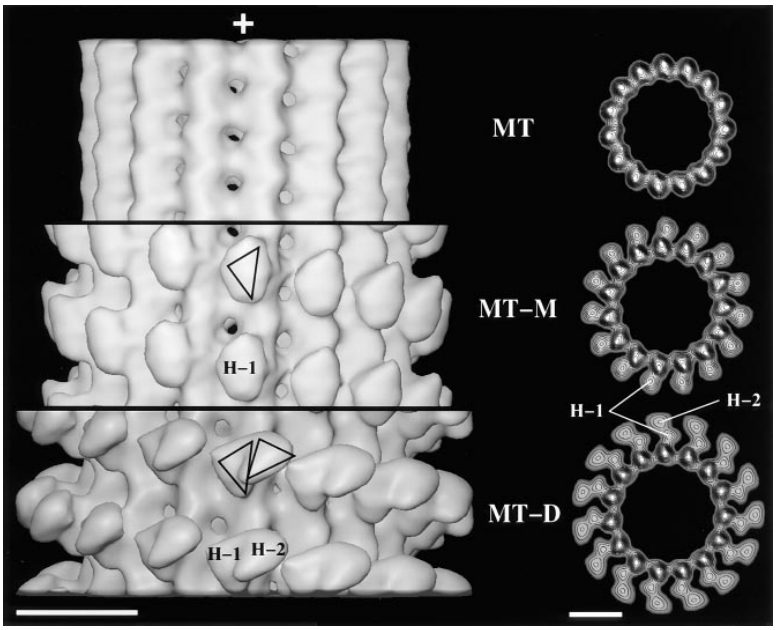

Figure 2. Three-Dimensional Maps

Surface representations (left) and end-on projections (right) of the 3-D maps of the undecorated microtubule (MT, top) and the microtubule decorated with monomeric (MT-M, center) and dimeric Ncd (MT-D, bottom). The surface representations are shown in side view and are oriented with the microtubule plus end at the top. The end projections represent the view from the plus end. In the MT-M and MT-D maps, triangles represent the motor domains associated with a single-tubulin heterodimer. H-1 (head 1) is the microtubule-attached head. H-2 is the detached head. Scale bars, 100 Å.

associated map densities as a consequence of data averaging, our results suggest that head 2 is firmly fixed in its orientation (see Arnal et al., 1996; Hirose et al., 1996). In the MT-D map, the contact area involving apposing faces of the two heads appears to be quite extensive, with the highest connecting map density lying toward the plus end of the microtubule. These observations suggest that the restraints on the position of head 2 may involve a specific interaction with head 1.

Combining EM and X-Ray Structures

To determine which parts of the Ncd motor domain interact with the microtubule, we systematically searched for the position and orientation of the Ncd motor domain crystal structure that best fits into the contours of 3-D maps of the microtubule–Ncd complexes calculated from cryo-EM images (Figure 3). The asymmetry and surface features of the motor domain in the 3-D maps and the fact that the N terminus must lie near the contact region between the two heads were the constraining parameters for the search. In order to minimize possible bias, the fitting was done independently by four individuals who had no knowledge of the results of Woehlke et al., 1997 (see accompanying paper, this issue of *Cell*). All the individuals determined an extremely similar orientation for the motor domain bound to the microtubule (head 1). The position of this motor was the same whether the fit was done on the MT-M map (Figure 3a) or the MT-D map (Figures 3b and 3c). The four fits differed from one another by a maximum of $\sim\pm5$ Å in position and $\sim\pm7°$ in rotation. This uncertainty does not affect our identification of the structural elements that are likely to participate in motor–microtubule interactions. The results of fitting the crystal structure into head 2 were somewhat equivocal. The less distinct morphology in the head 2 region of the 3-D map did not allow us to determine an unambiguous and unique fit. We currently favor the orientation shown in Figures 3b and 3c, but further work will be required for verification.

Several general features are evident from our model of the microtubule-bound head (head 1) (Figures 3 and 4a). First, the nucleotide-binding site is on the side of the motor domain opposite to the microtubule-binding face. Thus, the entrance to the nucleotide pocket is not sterically blocked by microtubule binding. Second, there is a good fit between the surface topographies of the apposing faces of the motor domain and the microtubule (Figure 4a). Finally, the N terminus of head 1 is close to and points in the direction of the density corresponding to head 2. In the dimer model shown in Figures 3b and 3c, the distance between the N termini of the two motor domains is $\sim$15 Å. The locations for the N termini are consistent with the fact that the Ncd dimer is held together by a coiled-coil domain that begins just N-terminal to the motor domain (McDonald and Goldstein, 1990).

Microtubule and Head–Head Interactions

In our model, the face of Ncd head 1, which is closely apposed to the microtubule, has four distinct regions that project toward the protofilament and are therefore leading candidates for the sites of motor–microtubule interaction (Figure 4). In the center of the face, there are two "arms" that seem to embrace the protofilament and make the closest contacts. Using the nomenclature of Sablin et al. (1996), loop 11 (L11) constitutes one arm. Contacts made by this arm are intriguing, since they occur in the groove between two microtubule protofilaments (Figures 3 and 4). The second arm is made up of secondary structure elements L12 and α4. The arms are separated from the other two regions of likely interaction by deep recesses in the motor domain that seem less likely to be part of the binding site. The third region of interaction is composed of L8 and lies toward the plus end of the microtubule (relative to the arms). The two arms and probably the L8 region bind to a single tubulin monomer (Figure 4a) and likely constitute what we have previously referred to as the major interaction between

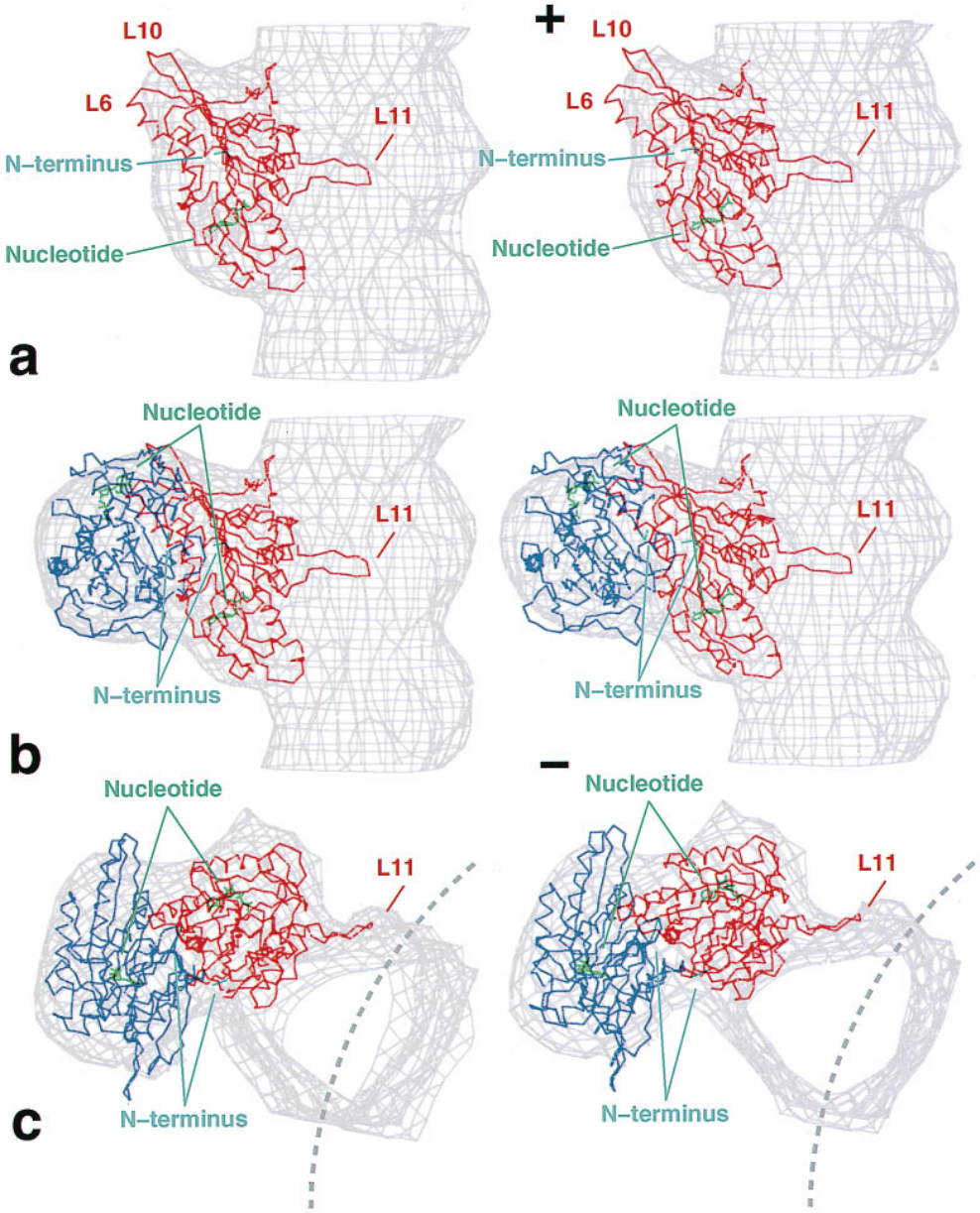

Figure 3. Stereo Views of the Ncd Crystal Structure Docked into the EM Maps

A side view of the Cα backbone of the Ncd motor domain (red) docked within the MT-M 3-D map (gray wire frame) is shown in (a). To help visualization of the fit between the motor domains and the three-dimensional maps, only the surface corresponding to one of the 15 protofilaments is displayed. The microtubule protofilament (pf) runs vertically with the plus end at the top. (b) shows the same view of the MT-D map with two Ncd motor domain Cα chains (red and blue) docked. In (c), the view is from the plus end. The locations of interprotofilament connections are identified by dotted lines. Secondary structure elements L6, L10, and L11 of the microtubule-attached Ncd head are indicated in (a).

the motor domain and the protofilament (Hoenger et al., 1995; Hoenger and Milligan, 1997). There is strong evidence indicating that this monomer is β tubulin (Fan et al., 1996; Hoenger and Milligan, 1996, 1997; Amos and Hirose, 1997). The fourth part of the binding site is made up of secondary structure elements L2 and α6. This region would correspond to the previously described minor interaction that spans the junction between adjacent tubulin monomers and makes contact with α tubulin (Hoenger and Milligan, 1997). Except for L2, all of these secondary structure elements are located in the C-terminal half of the motor domain. The presence of interactions with both tubulin subunits is in agreement with recent cross-linking experiments (Walker, 1995; Tucker and Goldstein, 1997).

The results in Figure 3 also suggest that regions surrounding L6 and L10 of head 1 project into the density of the second (detached) head. Although the crystal

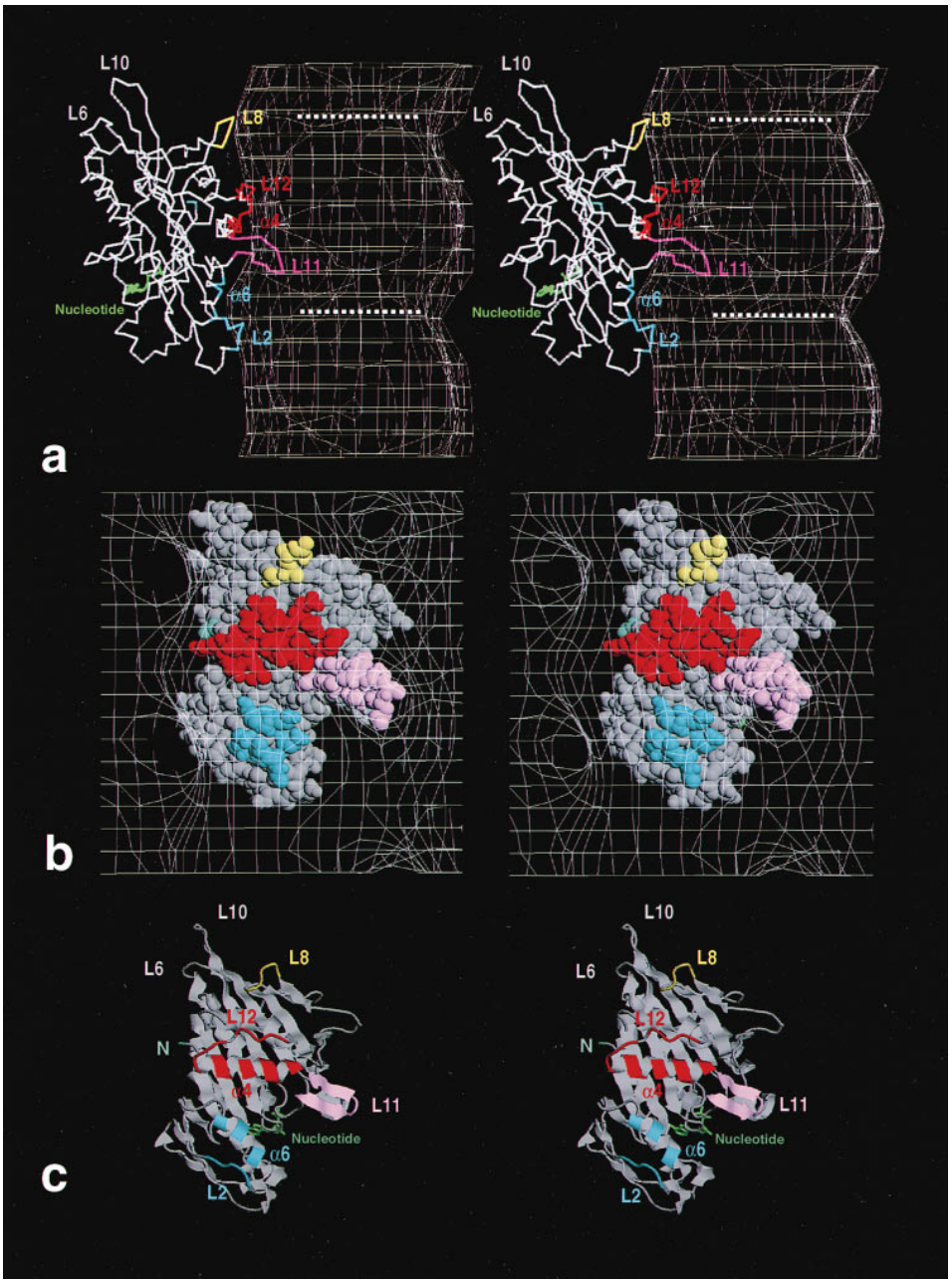

Figure 4. Stereo Views of the Model of the Attached Ncd Motor Domain Illustrating the Structural Elements Involved in Microtubule Binding

(a) Side view of a single protofilament from the MT map with the docked Ncd crystal structure. The center of the microtubule is at right. Estimated locations of the boundaries between tubulin monomers are indicated by dashed lines. Space-filling (b) and secondary-structure (c) representations of the attached Ncd motor domain viewed from within the tubulin protofilament. The overlying wire frame in (b) is the outer surface of the microtubule. In (a)–(c), the protofilament runs vertically with the plus end at the top. The four regions of the binding site are colored as follows: the L11 arm is pink, the L12-α4 arm is red, the plus end contact (L8) is yellow, and the minus end contact (L2-α6) is blue.

structure fit in head 2 is not certain, a close interaction with the L6-L10 region in head 1 is common to all the possible orientations we have identified. This suggests that residues in these loops and neighboring secondary structure elements may be involved in the head–head interactions that appear to be responsible for the relatively well-defined density of the detached head (head 2) in the 3-D map.

Discussion

In this study, we report the docking of an atomic structure of a kinesin family motor domain into 3-D density maps of a motor–microtubule complex determined by cryo-EM. The Ncd crystal structure fits well into the electron density of the microtubule-bound head without significant steric clashes between the motor and the

microtubule. This was not necessarily expected, since the bound nucleotide in the 3-D EM maps (AMP-PNP) is different in the crystal structure (ADP), and since the motor in the crystal is not interacting with tubulin. These results suggest that the motor catalytic core does not undergo very large shape changes between these two nucleotide states or between free and microtubule-bound states, at least as can be discerned at the resolution of this study.

There are several reasons for believing that the orientation of the microtubule-bound head is correct to within a few angstroms and a few degrees. First, the solution was derived from four independent fits and was the same for maps of Ncd monomers and dimers bound to microtubules. Second, the orientation places the N terminus of the catalytic core in close proximity to the second head, which is consistent with a proposed dimerization interaction via a coiled-coil structure adjacent to the motor domain (McDonald and Goldstein, 1990). Finally, as discussed below, the microtubule-binding regions identified in this study generally agree with those identified from an alanine-scanning mutagenesis analysis of the conventional kinesin motor domain reported by Woehlke et al. (1997).

The model in Figures 3 and 4 suggests that the interaction between Ncd and the microtubule protofilament is extensive and involves four regions of the motor domain: two centrally located "arms" (L11 and α4-L12) and a "plus-end contact" (L8) that make up the major interaction with the putative β tubulin monomer, and a "minus end contact" (L2-α6) that constitutes the minor interaction with the putative α tubulin (Fan et al., 1996; Hoenger and Milligan, 1996, 1997; Amos and Hirose, 1997). Although it should be noted that their close proximity to the microtubule does not necessarily indicate that all of these elements form strong contacts, the results presented here are generally consistent with the locations of functionally important residues in the microtubule-binding interface of the conventional kinesin motor domain as identified by alanine-scanning mutagenesis (Woehlke et al., 1997). For example, L12, which is closely docked onto the crest of the protofilament in our model, contains highly conserved, solvent-exposed residues, and proteins with alanine mutations in these residues have significantly decreased microtubule affinity. Also consistent with our structural model, mutations in L8, L11, α4, and α6 result in altered microtubule affinity. Mutations that alter microtubule affinity have not yet been identified in L2. However, it is interesting to note that L2 in Ncd contains ten more residues than the corresponding loop in conventional kinesin (Sablin et al., 1996) and thus extends closer to the microtubule in our model. It is possible that tubulin contacts in this loop differ among classes of kinesin motors and could play a role in directional movement, although further functional studies are required to explore this idea. The consistency of this study's findings on Ncd with those of the Woehlke et al. study on kinesin further suggest that the microtubule-binding interactions of these plus-end- and minus-end-directed motors are similar, in agreement with other biochemical (Lockhart et al., 1995) and structural (Amos and Hirose, 1997; Hoenger and Milligan, 1997) studies. Taken together, the mutagenesis and structural studies provide strong support for the identification of structural elements constituting the major interaction between the kinesin family motor domain and the underlying β tubulin monomer.

When the structures of kinesin and myosin were aligned, two large actin-binding domains in myosin were found to correspond topologically to L8 and L12 in kinesins, and it was speculated that these loops in kinesins might also serve as microtubule-binding sites (Kull et al., 1996; Sablin et al., 1996). Our model is consistent with this idea, but it also suggests that additional elements (L11, α4, α6, and L2) contribute to the microtubule-binding interface. Therefore, kinesins appear to have unique mechanisms of interacting with their polymer substrate that are not strictly analogous to those found in the actomyosin system. A unique and particularly notable structure is L11, the arm that extends into the groove between two microtubule protofilaments. The tip of L11 contains two conserved residues in the kinesin superfamily (M593 and E595 in Ncd), which are positioned deep in the groove. The location of this putative contact is intriguing, since it was speculated that kinesin motors may interact with the protofilament groove based upon the finding that kinesin interacts poorly with antiparallel protofilaments in tubulin zinc sheets (Ray et al., 1995). The importance of L11 is also suggested by the observations that residues in its N-terminal region are likely to contact the γ-phosphate of ATP in the active site (Kull et al., 1996), and that the loop is expected, on the basis of comparisons with other NTPases, to change conformation during ATP hydrolysis (Sablin et al., 1996). Therefore, L11 may be a unique region in kinesin motors that is important for polymer recognition and for communicating information between the microtubule- and nucleotide-binding sites.

Our observation that there is similar density associated with both the microtubule-bound head and the detached head in the 3-D maps indicates that there is a strong specific interaction between the two motor domains of the Ncd dimer. The position of the microtubule-bound head suggests that areas centered around two loops, L6 and L10, are candidates for mediating head–head interactions in the microtubule-bound motor. The locations of these loops are interesting, since they are located at the tip of the "arrowhead" structure of kinesin and Ncd motors. The arrowhead tip is composed of the ends of the longest helix in the motor (α2, which precedes L6) and three $\sim$10 amino-acid-long β-strands (β4, which follows after L6, and β6 and β7, which are connected by L10) that are unusually long compared to typical β strands in α/β proteins (6–7 residues) (Sablin et al., 1996). When the 13 secondary structural elements common to kinesin and myosin are compared, it is striking that α2, β4, β6, and β7 are the only ones that are significantly longer in kinesin compared with myosin (Kull et al., 1996). This observation suggests that the extended length of these elements may serve some unique function in kinesin motors, such as stabilization of head–head interactions.

Head–head interactions, as well as interactions involving regions outside the motor domain that join the two polypeptides together, could be important for defining the relative orientations of the two motor domains in the

microtubule-bound complex. The position of the detached head differs in microtubule-bound kinesin and Ncd dimers. In the case of Ncd, the detached head is oriented toward the microtubule minus end, while in kinesin, the equivalent head is positioned more toward the plus end (Arnal et al., 1996; Hirose et al., 1996). This difference may be important for directionality of movement, since the detached head would be better positioned to take a step toward a minus-end binding site for Ncd and a plus-end binding site for kinesin (Hackney, 1994). Interestingly, there are residues at or near the arrowhead tip that are conserved only within classes of related kinesin motors, and these may play some role in specifying unique head–head interactions and orientations of the detached head. Thus, our structural model suggests a new function for the "arrowhead tip" of kinesin motors, which can be further tested in functional assays.

Experimental Procedures

Chemicals and Proteins

HPLC-purified AMP-PNP was purchased from ICN (Irvine, CA). Taxol was purchased from Calbiochem-Novabiochem (La Jolla, CA). All other chemicals were of analytical grade. Bovine brain tubulin was obtained from CYTOSKELETON (Denver, CO). Monomeric Ncd (R335-K700) was prepared as described previously (Shimizu et al., 1995). Dimeric Ncd protein (D250-K700) was prepared as follows. A DNA fragment encoding 451 amino acids from Asp-250 to the C-terminal Lys of the Ncd protein was synthesized by PCR and cloned into a pHB40P translation vector using NdeI and XbaI restriction sites. The recombinant plasmid was transformed into BL21(DE-3)pLysE host cells for expression. Cells were grown at 24°C in 1 l of LB media supplemented with ampicillin (0.1 mg/l) to an OD_{600} of 0.3–0.4 and induced by addition of 0.2 mM IPTG for 8 hr at 24°C. Induced cells were frozen in liquid nitrogen and stored at −70°C. After thawing at 4°C, cells were resuspended in 40 ml of PB buffer (10 mM PIPES [pH 7.2], 80 mM NaCl, 2 mM $MgCl_2$, 1 mM EGTA, 1 mM DTT, and protease inhibitors) with 0.1 mg/ml DNAase I, and a cell lysate was made using a French pressure cell press (American Instrument Company). The cell lysate was centrifuged at 30,000 × g for 30 min, and the supernatant was loaded onto a 10 ml SP-Sepharose FF (Pharmacia) column that was equilibrated in PB. The column was washed with PB, and then a 100 ml linear NaCl gradient (0.1–0.3 M NaCl) was run to elute the Ncd from the column. The fractions containing the Ncd were pooled (20 ml), dialyzed against 1 l of TB buffer (10 mM Tris-HCl [pH 7.5], 80 mM NaCl, 2 mM $MgCl_2$, 1 mM EGTA, and protease inhibitors), and then loaded onto a FPLC MonoQ HR10/10 column (Pharmacia) equilibrated in TB. The column was washed with TB, and then a 80 ml linear NaCl gradient (0.1–0.2 M NaCl) was applied to elute the Ncd from the column. Pooled fractions containing >95% Ncd protein were concentrated to 5–6 mg/ml using a Centricon-30 (Amicon Inc.), frozen in liquid nitrogen, and stored at −70°C.

Sample Preparation

Microtubules were polymerized by incubating purified tubulin (2.5 mg/ml) in 80 mM PIPES [pH 6.8], 4 mM $MgCl_2$, 1 mM EGTA, 2 mM GTP, 5% DMSO, and 15 μM Taxol for 20 min at 37°C. Microtubule solution (4–5 μl) was applied to glow discharged, holey carbon support films on 400 mesh electron microscope grids. Decoration with Ncd motor domain was done on the grid by blotting away most of the microtubule solution and then applying 4–5 μl of Ncd motor protein solution (2 mg/ml Ncd in 10 mM Tris-HCl [pH 7], 67 mM NaCl, 2 mM $MgCl_2$, 1 mM DTT, and 4 mM AMP-PNP). Finally, the grids were blotted and frozen by rapidly plunging them into liquid ethane slush (Dubochet et al., 1988). Frozen grids were stored under liquid nitrogen. A Gatan (Pleasanton, CA) cryo-stage was used to maintain the grids below −180°C during transfer and observation in Philips CM120T or CM200T FEG electron microscopes. Electron micrographs were recorded under low dose conditions (<10 e/Å^2 total dose) at an operating voltage of 100 kV, nominal magnifications of 35,000 or 38,000, and an underfocus of 1–2 μm.

Image Analysis

Images of microtubules with 15 protofilaments (pf) whose diffraction patterns indicated that the tubulin dimers followed a 2-start helical path were chosen for analysis (Sosa et al., 1997). Selected micrographs were digitized on a Perkin-Elmer flatbed microdensitometer with spot and step sizes of 20 μm, equivalent to 5.26 Å or 5.71 Å at the specimen. In calculated diffraction patterns, the positions of the zeroes in the contrast transfer function (CTF) were determined, and the amplitudes and phases in the transform were then corrected, assuming 10% amplitude contrast. We further checked that the microtubules were helical by calculating 3-D maps by a backprojection method that does not assume helical symmetry (Wade et al., 1995; Sosa and Milligan, 1996). No seams were found in any of the 15 pf microtubules analyzed by backprojection. Thus, we concluded that under the polymerization conditions used, all 15 pf microtubules with a 2-start tubulin dimer path are helical. Subsequently, the images were analyzed by standard helical reconstruction procedures (DeRosier and Moore, 1970) on Silicon Graphics (Mountain View, CA) workstations using the software package PHOELIX (Whittaker et al., 1995; Carragher et al., 1996). Briefly, an integral number of microtubule moiré repeats (4–7) were masked off and Fourier transformed. Near- and far-side layer lines with Bessel orders up to ±30 and to an axial resolution of 1/18 Å^{-1} were extracted from the transform of each filament. For each of the final 3-D maps, all the corresponding data sets were averaged after bringing them to a common phase origin. Three cycles of origin refinement were carried out using the strongest layer lines (Bessel orders: 15, −2, 13, −4, 11). One of the raw data sets was used as a reference for the first phase origin refinement. In the second and third cycles, the average from the previous cycle was used as the new reference. The axial positions of the layer lines were then refined by two cycles of "sniffing" (Morgan and DeRosier, 1993). This procedure was repeated until no further improvement in the phase residuals was detected. The final sets of averaged layer lines were truncated at 1/18 Å^{-1}, and 3-D maps were calculated by Fourier-Bessel inversion. The polarity of the 3-D maps was determined from the characteristic polar features present in the tubulin part of the maps, e.g., the protofilament slew (see Sosa and Milligan, 1996).

Docking the Crystal Structure into the 3-D EM Maps

The position and orientation of the crystal structure of the motor domain of Ncd in the microtubule–Ncd 3-D maps were determined manually using the program O (Jones et al., 1991). To avoid bias, four individuals who were unaware of the results of Woehlke et al. (1997) did the fitting independently. The fits were carried out using both the MT-M and MT-D maps, and the same results were obtained for the microtubule-bound motor domain. Comparisons revealed that the various fits of the bound motor domain differed by only ∼±5 Å in position of the center of mass and ∼±7° in orientation. For the detached head (head 2), the structural details in the 3-D map were insufficient to allow determination of a unique fit. Further constraints will be needed before an unequivocal result can be obtained. Space-filling and secondary structure representations of the crystal structure were drawn with RasMol (Sayle and Milner-White, 1995).

Acknowledgments

We thank Bridget Carragher for help with computer programs. This work was supported by grants from the National Institutes of Health (GM52468 to R. A. M. and AR42895 to R. J. F. and R. D. V.), a Human Frontier Science Program Fellowship (LT-619/94 to A. H.), a Leukemia Society of America postdoctoral fellowship (to E. S.), and an American Heart Association predoctoral fellowship (to D. P. D.). R. A. M. is an Established Investigator of the American Heart Association.

Received April 14, 1997; revised June 12, 1997.

References

Amos, L.A., and Hirose, K. (1997). The structure of microtubule-motor complexes. Curr. Opin. Cell Biol. *9*, 4–11.

Amos, L.A., and Klug, A. (1974). Arrangement of subunits in flagellar microtubules. J. Cell Sci. *14*, 523–549.

Arnal, I., Metoz, F., DeBonis, S., and Wade, R.H. (1996). Three-dimensional structure of functional motor proteins on microtubules. Curr. Biol. *6*, 1265–1270.

Bloom, G.S., and Endow, S.A. (1995). Motor proteins 1: kinesins. Protein Profile *2*, 1105–1171.

Carragher, B.O., Whittaker, M., and Milligan, R.A. (1996). Helical processing using PHOELIX. J. Struct. Biol. *116*, 107–112.

Chrétien, D., and Wade, R.H. (1991). New data on the microtubule surface lattice. Biol. Cell *71*, 161–174.

DeRosier, D.J., and Moore, P.B. (1970). Reconstruction of three-dimensional images from electron micrographs of structures with helical symmetry. J. Mol. Biol. *52*, 355–369.

Dubochet, J., Adrian, M., Chang, J.J., Homo, J.-C., Lepault, J., McDowall, A.W., and Schultz, P. (1988). Cryo-electron microscopy of vitrified specimens. Quart. Rev. Biophys. *21*, 129–228.

Fan, J., Griffiths, A.D., Lockhart, A., Cross, R., and Amos, L. (1996). Microtubule minus ends can be labelled with a phage display antibody specific to alpha-tubulin. J. Mol. Biol. *259*, 325–330.

Hackney, D.D. (1994). Evidence for alternating head catalysis by kinesin during microtubule stimulated ATP hydrolysis. Proc. Natl. Acad. Sci. USA *91*, 6865–6890.

Hirose, K., Lockhart, A., Cross, R.A., and Amos, L.A. (1996). Three-dimensional cryoelectron microscopy of dimeric kinesin and Ncd motor domains on microtubules. Proc. Natl. Acad. Sci. USA *93*, 9539–9544.

Hoenger, A., and Milligan, R.A. (1996). Polarity of 2-D and 3-D maps of tubulin sheets and motor-decorated sheets. J. Mol. Biol. *263*, 114–119.

Hoenger, A., and Milligan, R.A. (1997). Motor domains of kinesin and Ncd interact with microtubule protofilaments with the same binding geometry. J. Mol. Biol. *265*, 553–564.

Hoenger, A., Sablin, E.P., Vale, R.D., Fletterick, R.J., and Milligan, R.A. (1995). Three-dimensional structure of a tubulin-motor-protein complex. Nature *376*, 271–274.

Howard, J. (1996). The movement of kinesin along microtubules. Annu. Rev. Physiol. *58*, 703–729.

Jones, T.A., Zou, J.Y., Cowan, S.W., and Kjeldgaard, M. (1991). Improved methods for building protein models in electron density maps and the location of errors in these models Acta Cryst. *A47*, 110–119.

Kikkawa, M., Ishikawa, T., Wakabayashi, T., and Hirokawa, N. (1995). Three-dimensional structure of the kinesin head-microtubule complex. Nature *376*, 274–277.

Kull, F.J., Sablin, E.P., Lau, R., and Fletterick, R.J. (1996). Crystal structure of the kinesin motor domain reveals a structural similarity to myosin. Nature *380*, 550–555.

Lockhart, A., Crevel, I.M., and Cross, R.A. (1995). Kinesin and Ncd bind through a single head to microtubules and compete for a shared MT binding site. J. Mol. Biol. *249*, 763–771.

Mandelkow, E.-M., and Mandelkow, E. (1985). Unstained microtubules studied by cryo-electron microscopy: substructure, supertwist and disassembly. J. Mol. Biol. *181*, 123–135.

McDonald, H.B., and Goldstein, L.S.B. (1990). Identification and characterization of a gene encoding a kinesin-like protein in Drosophila. Cell *61*, 991–1000.

McDonald, H.B., Stewart, R.J., and Goldstein, L.S.B. (1990). The kinesin-like Ncd protein of Drosophila is a minus end-directed microtubule motor. Cell *63*, 1159–1165.

Moore, J.D., and Endow, S.A. (1996). Kinesin proteins: a phylum of motors for microtubule-based motility. Bioessays *18*, 207–219.

Morgan, D., and DeRosier, D. (1993). Detection of high resolution signal in electron micrographs of helices. Biophys. J. *64*, A243.

Ray, S., Wolf, S.G., Howard, J., and Downing, K.H. (1995). Kinesin does not support the motility of zinc-macrotubes. Cell Motil. Cytoskel. *30*, 146–152.

Rayment, I., Holden, H.M., Whittaker, M., Yohn, C.B., Lorenz, M., Holmes, K.C., and Milligan, R.A. (1993). Structure of the actin-myosin complex and its implications for muscle contraction. Science *261*, 58–65.

Rayment, I., Smith, C., and Yount, R.G. (1996). The active site of myosin. Annu. Rev. Physiol. *58*, 671–702.

Sablin, E.P., Kull, F.J., Cooke, R., Vale, R.D., and Fletterick, R.J. (1996). Crystal structure of the motor domain of the kinesin-related motor Ncd. Nature *380*, 555–559.

Sayle, R.A., and Milner-White, E.J. (1995). RasMol: biomolecular graphics for all. Trends Biochem. Sci. *20*, 374–376.

Shimizu, T., Sablin, E., Vale, R.D., Fletterick, R., Pechatnikova, E., and Taylor, E.W. (1995). Expression, purification, ATPase properties and microtubule binding properties of the Ncd motor domain. Biochemistry *34*, 13259–13266.

Sosa, H., and Milligan, R.A. (1996). Three-dimensional structure of Ncd-decorated microtubules obtained by a back-projection method. J. Mol. Biol. *260*, 743–755.

Sosa, H., Hoenger, A., and Milligan, R.A. (1997). Three different approaches for calculating the three dimensional structure of microtubules decorated with kinesin motor domains. J. Struct. Biol. *118*, 149–158.

Stewart, R.J., Thaler, J.P., and Goldstein, L.S.B. (1993). Direction of microtubule movement is an intrinsic property of the motor domains of kinesin heavy chains and Drosophila Ncd protein. Proc. Natl. Acad. Sci. USA *90*, 5209–5213.

Tucker, C., and Goldstein, L.S.B. (1997). Probing the kinesin-microtubule interaction. J. Biol. Chem. *272*, 9481–9488.

Vale, R.D., Schnapp, B.J., Mitchison, T., Steuer, E., Reese, T.S., and Sheetz, M.P. (1985). Different axoplasmic proteins generate movement in opposite directions along microtubules in vitro. Cell *43*, 623–632.

Wade, R.H., Horowitz, R., and Milligan, R.A. (1995). Towards understanding the structure and interactions of microtubules and motor proteins. Proteins *23*, 502–509.

Walker, R.A. (1995). Ncd and kinesin motor domains interact with both α- and β-tubulin subunits. Proc. Natl. Acad. Sci. USA *92*, 5960–5964.

Walker, R.A., Salmon, E.D., and Endow, S.A. (1990). The Drosophila claret segregation protein is a minus end-directed motor molecule. Nature *347*, 780–782.

Whittaker, M., Carragher, B.O., and Milligan, R.A. (1995). PHOELIX: A package for semi-automated helical reconstruction. Ultramicroscopy *58*, 245–259.

Woehlke, G.E., Ruby, A.K., Hart, C., Bernice, L., Hom-Booher, N., and Vale, R.D. (1997). Microtubule interaction site of the kinesin motor. Cell, this issue, *90*, 207–216.

Yang, J.T., Laymon, R.A., and Goldstein, L.S.B. (1989). A three-domain structure of kinesin heavy chain revealed by DNA sequence and microtubule binding analyses. Cell *56*, 879–889.

Yang, J.T., Saxton, W.M., Stewart, R.J., Raff, E.C., and Goldstein, L.S.B. (1990). Evidence that the head of kinesin is sufficient for force generation and motility in vitro. Science *249*, 42–47.